

An Illustration and Analysis of the Degeneracy in the Search for the Leptonic CP -Violating Phase and the Neutrino Mass Hierarchy

Masafumi KOIKE^{*)} and Masako SAITO^{**)}

Physics Department, Saitama University, Saitama 338-8570, Japan

Determination of the value of the leptonic CP -violating phase δ and the neutrino mass hierarchy $\text{sgn } \delta m_{31}^2$ through long baseline neutrino oscillation experiments is systematically analyzed. We note that the two oscillation spectra are difficult to discriminate and lead to the degeneracy when they are peaked at the same energy and have the same peak probability. The condition of peak-matching is therefore introduced as a criterion for the presence of degeneracy. The matching of peaks is visualized as an intersection of trajectories traced by the peak of an oscillation spectrum while the value of δ is varied from 0 to 2π . We numerically calculate a pair of trajectories for a pair of hierarchies and examine the degeneracy, especially that concerning the hierarchy. We formulate the trajectory in terms of analytic expressions and evaluate the critical length, which is shown to be proportional to $1/\sin \theta_{13}$. In view of our analysis, we discuss future prospects to solve the hierarchy degeneracy with regard to the following four approaches: elongating the baseline length sufficiently, using both neutrinos and anti-neutrinos, combining experiments with different baseline lengths, and observing two or more oscillation peaks.

§1. Introduction

Experiments suggest the existence of oscillation among the different flavors of neutrinos, providing rich information on the flavor structure of the lepton sector.^{1)–4)} Despite this progress, however, present knowledge of neutrinos is still incomplete. In the notation of Ref. 5), the values of the mass parameters and the mixing parameters yet to be determined include one of the mixing angles θ_{13} , the sign of δm_{31}^2 , and the CP -violating phase δ . The value of θ_{13} is confined only by an upper bound as $\sin^2 2\theta_{13} < 0.19$,⁵⁾ while the sign of δm_{31}^2 and the value of δ are completely unknown to date. CP violation manifests itself only in the flavor-changing appearance channel such as $\nu_\mu \rightarrow \nu_e$, which in turn is suppressed by a small factor of $\sin^2 2\theta_{13}$. For this reason, we expect a two-staged program in pursuing the unknown properties of neutrinos. The first stage is the search for θ_{13} . It is anticipated that its upper bound will be improved down to $\sin^2 2\theta_{13} \lesssim O(10^{-2})$ by planned experiments using nuclear reactors⁶⁾ and accelerators.⁷⁾ The second stage is the search for the sign of δm_{31}^2 and for CP violation. The next generations of long baseline neutrino oscillation experiments offer promising opportunities for such searches,⁷⁾ and other probes of the sign of δm_{31}^2 are also discussed in the literature.⁸⁾

Our focus in this paper is on the second stage based on the optimistic expectation that the next generation of reactor neutrino experiments will find evidence of non-vanishing θ_{13} and that its value will turn out to be large enough for the CP -violation search. We consider the search for the CP -violating phase and the sign of δm_{31}^2

^{*)} E-mail: koike@krishna.th.phy.saitama-u.ac.jp

^{**)} E-mail: msaito@krishna.th.phy.saitama-u.ac.jp

through long baseline neutrino oscillation experiments using a conventional beam of muon neutrinos. A single long-baseline experiment, however, does not necessarily lead to the determination of a unique set of values of oscillation parameters. One obstacle is the ambiguity of parameter values due to the experimental errors.^{9),10)} Another is the parameter degeneracy, which arises when the experimental results can be attributed to two or more sets of parameter values. Three types of the degeneracy are customarily referred to: the intrinsic degeneracy, on $(\theta_{13}, \delta_{CP})$;¹¹⁾ the hierarchy degeneracy, on $\delta m_{31}^2 \gtrless 0$;¹²⁾ and the octant degeneracy, on $\theta_{23} \gtrless \pi/4$.¹³⁾ Although the parameter degeneracy should be avoided,^{11)–16)} its presence is difficult to predict comprehensively due to the complicated dependence of experimental results on many parameters and on various setups of experiments. The plot introduced in Ref. 12) gives an overview of the presence of degeneracy and has been found versatile for its analysis. It presents the two oscillation probabilities or event rates of two channels in a two-dimensional space, enabling to show separately the CP -violating effect and the matter effect.

We introduce another aspect of the analysis of the energy spectrum of the appearance probability. Giving an intuitive illustration of the determination of the parameters from this spectrum, we offer a view of ours on the emergence of degeneracy and its resolution. The pivot of our study is the peak of the oscillation probability, particularly its position, or the energy and probability at the peak. We note that two oscillation spectra whose peak positions coincide are difficult to distinguish and likely to cause degeneracy. We trace the peak position varying the values of δ and $\text{sgn } \delta m_{31}^2$ to show how their search is entangled and the hierarchy degeneracy results. We vary the baseline length as well and describe from our point of view how the degeneracy disappears when the baseline becomes sufficiently long. We organize these analyses by deriving analytic expressions of the oscillation probability at the peaks and offer an overview concerning the presence of degeneracy and possible ways to avoid it.

The outline of this paper is as follows. In §2, we introduce the peak-matching condition as a criterion for the presence of degeneracy and facilitate its visualization by drawing closed trajectories of the oscillation peak. In §3, we develop an understanding of the presence and absence of the degeneracy of parameters through the loops of the peak. In §4, we derive an analytic expression of the $\nu_\mu \rightarrow \nu_e$ appearance probability at the oscillation peaks to elucidate its dependence on the mass parameters and the mixing parameters, and show how the loops are distorted due to the change of the baseline length. In §5, we apply the peak loops to the evaluation of four methods to uniquely determine the value of the CP -violating phase and the mass hierarchy. Section 6 presents the conclusion and discussion.

§2. Peak-matching condition and the peak loop

We assume that there are three neutrino generations and adopt the definitions given in Ref. 5) of the quadratic mass differences δm_{ij}^2 ($\{i, j\} \subset \{1, 2, 3\}$), the mixing angles θ_{ij} , and the CP -violating phase δ . All experimental results obtained to this time can be accounted for by neutrino oscillation by taking $\delta m_{21}^2 \simeq (8.0_{-0.3}^{+0.4}) \times$

10^{-5} eV^2 , $|\delta m_{31}^2| \simeq (1.9-3.0) \times 10^{-3} \text{ eV}^2$, $\sin^2 2\theta_{12} = 0.86_{-0.04}^{+0.03}$, $\sin^2 2\theta_{23} > 0.92$, and $\sin^2 2\theta_{13} < 0.19$,⁵⁾ with the exception of the LSND experiment,¹⁷⁾ whose results were not confirmed by either the KARMEN experiment¹⁸⁾ or the MiniBooNE experiment.¹⁹⁾ We do not take account of the ambiguities of these parameters in this paper for the sake of a clear presentation of our idea. The influence of these ambiguities will be discussed in §6.

We consider the search for the CP -violating phase δ and the mass hierarchy $\text{sgn} \delta m_{31}^2$ by investigating the $\nu_\mu \rightarrow \nu_e$ appearance probability in long baseline neutrino oscillation experiments. We do not treat the disappearance channel, which is effective in practical analyses to restrict parameter values such as the absolute value of δm_{31}^2 . Let us first illustrate with an example that the $\nu_\mu \rightarrow \nu_e$ appearance probability enables to search the value of δ and the sign of δm_{31}^2 . In Fig. 1, we display the $\nu_\mu \rightarrow \nu_e$ appearance probabilities in a case of a baseline length of $L = 700 \text{ km}$. There, the value of δ and the sign of δm_{31}^2 are varied while other parameters are fixed to a set of example values:

$$\delta m_{21}^2 = 8.2 \times 10^{-5} \text{ eV}^2, \quad (2.1a)$$

$$|\delta m_{31}^2| = 2.5 \times 10^{-3} \text{ eV}^2, \quad (2.1b)$$

$$\sin^2 2\theta_{12} = 0.84, \quad (2.1c)$$

$$\sin^2 2\theta_{23} = 1.0, \quad (2.1d)$$

$$\sin^2 2\theta_{13} = 0.06. \quad (2.1e)$$

The matter density ρ on the baseline is assumed to be constant and fixed to

$$\rho = 2.6 \text{ g/cm}^3, \quad (2.1f)$$

which is related to the electron number density n_e as $n_e = N_A Y_e \rho$ with the Avogadro constant N_A and the proton-to-nucleon ratio Y_e on the baseline. For convenience, we use this set of values and assume $Y_e = 0.5$ for the numerical calculations in this paper unless otherwise noted. Figure 1 plots the energy spectra of the appearance probability (a) for $\delta m_{31}^2 = +2.5 \times 10^{-3} \text{ eV}^2 > 0$ (normal hierarchy) and (b) for $\delta m_{31}^2 = -2.5 \times 10^{-3} \text{ eV}^2 < 0$ (inverted hierarchy). Figure 1(c) displays two spectra for the set of parameter values given in it. We can clearly see the dependence of the spectrum upon δ and $\text{sgn} \delta m_{31}^2$ in (a) and (b), and thus we can search for these values through $\nu_\mu \rightarrow \nu_e$ appearance experiments.

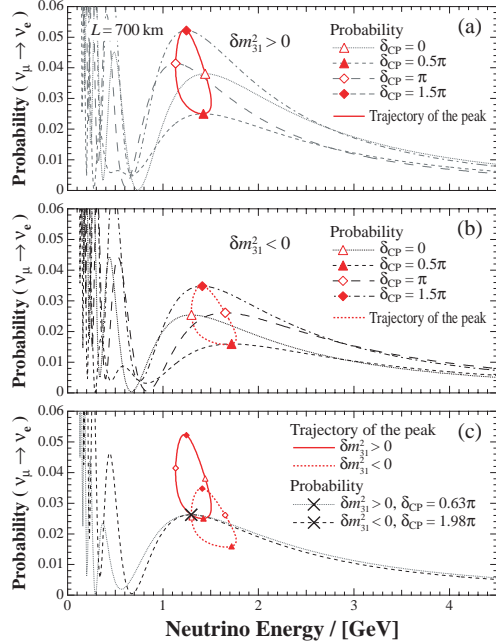


Fig. 1. The $\nu_\mu \rightarrow \nu_e$ appearance probabilities and the trajectories of their first peaks for a baseline length of 700 km. The parameter values in Eq. (2.1) are adopted. Figure (a) is for the normal hierarchy and Fig.(b) is for the inverted. Each includes the probability spectra for $\delta = 0, \pi/2, \pi$ and $3\pi/2$. Figure (c) overlays the trajectories of the top two, along with two oscillation spectra peaked at the intersection of these trajectories marked by the “x” symbol.

This dependence, however, does not guarantee that we can uniquely determine these values from a single experiment. Experimental results in some cases are consistent with both normal and inverted hierarchies, each with an appropriate choice of the value of δ . For example, an experiment providing the oscillation spectrum of the dashed curve in Fig. 1(c) would reject neither $(\text{sgn } \delta m_{31}^2, \delta) = (+, 0.63\pi)$ nor $(\text{sgn } \delta m_{31}^2, \delta) = (-, 1.98\pi)$ and leads to the hierarchy degeneracy, if the low-energy neutrinos below about 1 GeV are unobservable. The degeneracy introduces unfavorable complication into the analysis and should be avoided.

We now direct our attention to the peak of the appearance probability spectrum since it gives insight into the presence of hierarchy degeneracy. An appearance probability has a series of peaks $(E_{\text{peak},n}, P_{\text{peak},n})$ ($n = 0, 1, 2, \dots$) with $E_{\text{peak},0} > E_{\text{peak},1} > E_{\text{peak},2} > \dots$. Each peak traces out a closed trajectory as we vary the value of δ from 0 to 2π , keeping the other parameters fixed. The loops traced by the first peak ($n = 0$) are presented in Fig. 1(a) for $\delta m_{31}^2 > 0$ and (b) for $\delta m_{31}^2 < 0$. The peak positions for $\delta = 0, \pi/2, \pi$, and $3\pi/2$ are indicated on the loops by open triangles, solid triangles, open diamonds, and solid diamonds, respectively. We observe that the peak position for the normal (inverted) hierarchy moves clockwise (counterclockwise) on the loop as the value of δ increases.

In Fig. 1(c), the peak loops for $\delta m_{31}^2 \gtrless 0$ are copied from Figs. 1(a) and (b) with the symbol “ \times ” marking one of their intersections. This intersection corresponds to the two sets of parameter values given in the figure. With these values, the shown oscillation probabilities are both peaked at the symbol as should be the case. We observe the similarity of the two for $E \gtrsim 1$ GeV despite their difference for lower energies. Given the typical visible energy of neutrinos $E > (0.5 - 1.0)$ GeV, we expect that their similarity will make it difficult to distinguish the two sets of parameter values by experiments and thus lead to degeneracy.

We arrive here at an intuitive understanding of the presence of degeneracy. Assume that the visible energy range of an experiment covers a peak $(E_{\text{peak},n}, P_{\text{peak},n})$ of the appearance probability. (In §5 we discuss cases in which two or more peaks are visible, which occurs when a sufficiently long baseline, typically $L \gtrsim 1000$ km, and a wide-band neutrino beam are used.) The values of $E_{\text{peak},n}$ and $P_{\text{peak},n}$ depend on the oscillation parameters such as δm_{ij}^2 , θ_{ij} , and δ , which we collectively denote by $\{\vartheta_i\}$. The observation made in the previous paragraph signifies that the two parameter sets $\{\vartheta_i\}$ and $\{\vartheta'_i\}$ will be degenerate when the peak-matching condition

$$E_{\text{peak},n}(\{\vartheta_i\}) = E_{\text{peak},n}(\{\vartheta'_i\}), \quad (2.2a)$$

$$P_{\text{peak},n}(\{\vartheta_i\}) = P_{\text{peak},n}(\{\vartheta'_i\}) \quad (2.2b)$$

is satisfied. This condition was first tested in Ref. 10) in the analysis of an example study, although not extensively. In particular, the hierarchy degeneracy arises when the values of δm_{31}^2 in $\{\vartheta_i\}$ and in $\{\vartheta'_i\}$ have opposite signs.

We confirm the validity of the intuitive discussion above by carrying out a quantitative comparison of the two spectra shown in Fig. 1(c), following the analysis given in Sec. III A of Ref. 10). Our analysis assumes the neutrino beam flux shown in Fig. 2, which is the spectrum of the wide-band neutrino beam expected from the upgraded Alternate Gradient Synchrotron at Brookhaven National Laboratory in

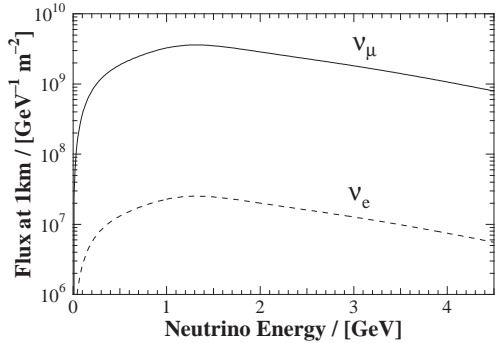


Fig. 2. The neutrino fluxes used in the example analysis. The flux of muon neutrinos (solid curve) is the spectrum of the wide-band neutrino beam expected from the upgraded Alternate Gradient Synchrotron at Brookhaven National Laboratory.²⁰⁾ The flux of electron neutrinos (dotted curve) is assumed to be 0.7% of that of muon neutrinos with the same energy dependence.

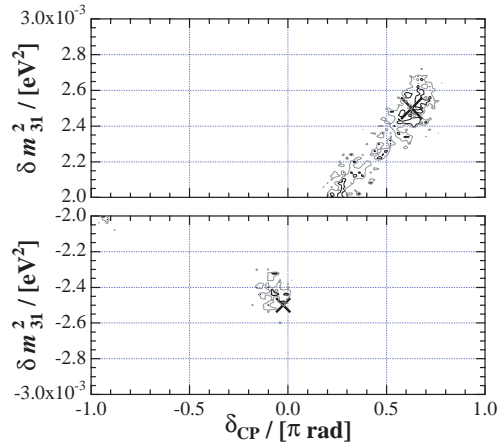


Fig. 3. Allowed regions for 68.3% (gray curve) and 95% (black curve) confidence levels obtained from an example χ^2 analysis of the $\nu_\mu \rightarrow \nu_e$ appearance events between 0.7 GeV and 4.1 GeV. The large “x” symbol in the top figure indicates the true parameter values of our choice and the small one in the bottom indicates the peak-matching partner of the true values as explained in the text.

the U.S.A.²⁰⁾ This flux is suitable for the present example where we continue to use $L = 700$ km, since its maximal energy $E \simeq (1-2)$ GeV coincides with the first-peak energy of the oscillation probability at this distance for $|\delta m_{31}^2| \simeq (2-3) \times 10^{-3} \text{ eV}^2$. We also assume a water Čerenkov detector with a fiducial mass of 500 kt and a data acquisition time of 5×10^7 s. Other details of the setups are the same as in Ref. 10). The analysis is briefly outlined as follows. We fix the set of “true” parameter values as $(\delta m_{31}^2, \delta) = (+2.5 \times 10^{-3} \text{ eV}^2, 0.63\pi)$ taken from Fig. 1(c), along with the values in Eq. (2.1). The “test” values of δ and δm_{31}^2 are varied over the parameter space while other parameters are fixed to their true values. We generate an energy spectrum for this test value and check its consistency with the true value via a χ^2 goodness-of-fit analysis. The test values that pass this check constitute the allowed region. Figure 3 shows the allowed regions with 68.3% and 95% confidence levels obtained from the χ^2 analysis over the range $0.7 \text{ GeV} < E < 4.1 \text{ GeV}$. The top graph is for the normal hierarchy, and the bottom for the inverted. The large “x” symbol on the top graph indicates the true values of the parameters, and the allowed region extends around it due to statistical error, systematic error, and the background. Also in the bottom graph is the allowed region, which indicates the presence of a hierarchy degeneracy. The small “x” symbol located at $(\delta m_{31}^2, \delta) = (-2.5 \times 10^{-3} \text{ eV}^2, -0.02\pi)$ indicates the peak-matching partner of the true value of our choice shown in Fig. 1(c) as $-0.02\pi \equiv 1.98\pi \text{ mod } 2\pi$. Note that it falls just within the allowed region with the wrong hierarchy, indicating the degeneracy of the two sets of parameter values.

§3. Degeneracy in light of the peak loops

We showed in the previous section that the degeneracy follows from the two parameter sets which bring the oscillation peak to the same position. We employ the peak loops in this section to present a simple understanding of the presence of the degeneracy.

3.1. Emergence of degeneracy: case studies

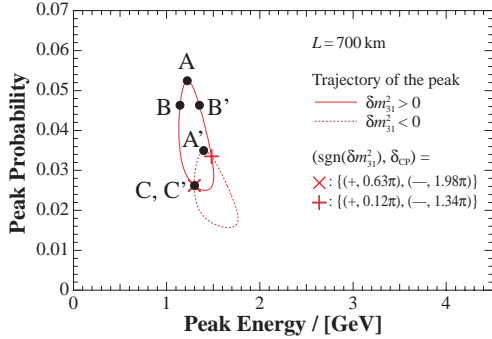


Fig. 4. Trajectories of the first oscillation peak for the baseline length of 700 km. The oscillation parameters in Eq. (2.1) are adopted. The solid curve is for the normal hierarchy and the dotted one for the inverted. The “x” and “+” symbols denote the intersections of the trajectories. The points of A, A’, B, B’, C, and C’ are referred to in the text.

Sufficient precision and accuracy are necessary to put the determination into practice. Even well-controlled experiment, however, can fail to determine uniquely the parameter values if the true peak falls right upon an intersection of the loops, giving two possible sets of values as seen in Eq. (3.1). We demonstrate how degeneracies emerge in three typical cases where the true peak is at the points A, B, and C in Fig. 4.

Case (A): The true hierarchy is normal and the true oscillation peak is at the point A in Fig. 4. Owing to the vertical separation of the two loops, the sign of δm_{31}^2 is determined as positive once the appearance probability is determined precisely enough to distinguish the point A from the point A’. The value of δ is restricted to a single allowed region around the value for A and the size of this region depends on the experimental precision and accuracy.

Case (B): The true hierarchy is normal and the true oscillation peak is at the point B in Fig. 4. The value of δ is constrained to a single allowed region as in the previous case if the energy resolution of the experiment is high enough to distinguish the points B and B’ on the parallel sides of the loop. If, on the other hand, the resolution is not sufficient, the values of δ for B and for B’ become indistinguishable

We explain how we can read the presence and absence of the hierarchy degeneracy from the peak loops introduced in the previous section. In Fig. 4, we reproduce the pair of peak loops presented in Fig. 1(c). The upper loop for $\delta m_{31}^2 > 0$ and the lower loop for $\delta m_{31}^2 < 0$ intersect at two points, each of which gives a pair of values of $(\text{sgn } \delta m_{31}^2, \delta)$; in this example the two pairs are

$$\begin{aligned} & \{(+, 0.63\pi), (-, 1.98\pi)\}, \\ & \{(+, 0.12\pi), (-, 1.34\pi)\}. \end{aligned} \quad (3.1)$$

The true values of $(\text{sgn } \delta m_{31}^2, \delta)$ provided by Nature give an oscillation spectrum whose first peak falls on some point on the two loops. We can correctly determine these values by identifying this point through experiments.

and the allowed region will extend around these two values.

Case (C): The true hierarchy is normal, and the true oscillation peak is at the point C, which is the intersection of the two loops. There exists another value of δ that brings the oscillation peak to the same point C' but with the inverted hierarchy, and we are thus led to a hierarchy degeneracy. Here we regard the points C and C' to be on the upper and lower loops, respectively, in spite of their coincident positions. The allowed region consists of two separate parts which extend around the parameters for C and for C'.

3.2. Degeneracy in varying the baseline length

Next we examine how a pair of loops move and become distorted as we vary the baseline length of the neutrino oscillation experiments. We present in Fig. 5 peak loops obtained as we vary the baseline length from 300 km to 1500 km, while fixing the other parameters to the example values given in Eq. (2.1). For a relatively short baseline ($L \sim 300$ km in our example), the loop for the normal hierarchy (the “normal loop”) and for the inverted hierarchy (the “inverted loop”) have similar shapes and overlap each other significantly. As the baseline becomes longer, the normal loop and the inverted loop move upward and downward, respectively, and they diverge due to the matter effect. The inverted loop is at the same time appreciably stretched in the E -direction and flattened in the P -direction. The two loops are seen to become disjoint at a certain baseline length. This critical length L_{crit} for the present parameter set is $L_{\text{crit}} \simeq (1100 - 1300)$ km as can be read in Fig. 5.

From the above observations, we reach following outlook upon the determination of the hierarchy and the CP -violating phase.

The hierarchy is difficult to determine by experiments with a short baseline length where the pair of loops overlaps considerably. We expect, however, that the hierarchy can be determined when the true peak is located at the top part of the upper loop or at the bottom part of the lower loop. The determination of the hierarchy becomes easier as the baseline becomes longer and as the increasing effect of the matter separates the pair of loops. When the baseline is longer than the critical length, the condition given in Eq. (2.2) is never satisfied with opposite hierarchies and the hierarchy can thus be uniquely determined regardless of the value of δ .

The search for the value of δ is entangled with that for the hierarchy. The hierarchy degeneracy is one obstacle to the determination of the value of δ especially when the baseline is short. Another obstacle is the experimental limitation on the

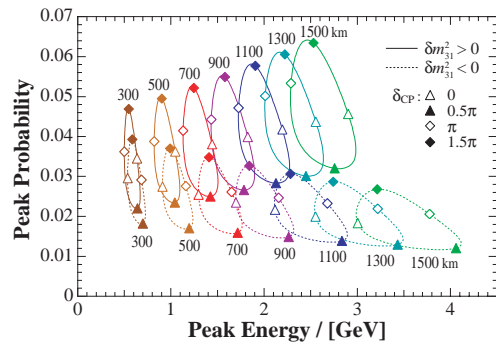


Fig. 5. Trajectories of the first oscillation peak for baseline lengths between 300 km and 1500 km. The oscillation parameters in Eq. (2.1) are adopted. The solid curve is for the normal hierarchy and the dotted one for the inverted.

energy resolution and on the precision and the accuracy of the oscillation probability. The loop is narrow in the E -direction when the baseline is short, and the resolution of the energy must be sufficiently high to distinguish the parallel sides of the loops; otherwise an additional degeneracy will be introduced. In contrast, the inverted loop is flattened in the P -direction when the baseline is long. We thus require precise and accurate measurements of the oscillation probability to avoid introducing an extra degeneracy.

§4. Analytic study of the peak loops

We have illustrated the determination of parameters with the aid of peak loops and found their position, size, and shape informative. In this section, we exploit analytic expressions of the oscillation probability to formulate them in terms of the mass parameters, the mixing parameters, and the baseline length. We thereby analyze how a pair of peak loops for $\delta m_{31}^2 \gtrsim 0$ are distorted and separated as the baseline length increases.

4.1. Formulation of the peak loops via the oscillation probability formula

We derive formulae for the oscillation probability with a perturbative expansion of the S -matrix in terms of $\Delta_{21} \equiv \delta m_{21}^2 L/2E$ and $\Delta_m \equiv \sqrt{2}G_F n_e L$, where $G_F = 1.166 \times 10^{-5} \text{ GeV}^{-2}$ is the Fermi constant. The derivation was first worked out to first order to analyze the effect of CP violation separately from the matter effect.²¹⁾ In the present paper, we calculate the $\nu_\mu \rightarrow \nu_e$ appearance probability to second order with the following consideration. Note that a peak loop collapses to a point when δm_{21}^2 vanishes since CP violation is a three-generation effect. The size of the peak loop is thus of first order, and its distortion depending on the baseline length, in which we are interested, is of second order or higher. The second-order calculation outlined in Appendix A results in lengthy expressions and we apply an additional simplification that exploits the smallness of θ_{13} . We drop $O(\sin^2 \theta_{13})$ terms in the coefficients of Δ_{21}^2 and $\Delta_m \Delta_{21}$, as well as $O(\sin^3 \theta_{13})$ terms in that of Δ_m^2 . Here we take account of the relation $\Delta_m > \Delta_{21}$, which holds for the cases in which we are interested (see Appendix B). We then obtain

$$P(\nu_\mu \rightarrow \nu_e, E) = 4l(A \sin^2 \Theta + B), \quad (4.1a)$$

where

$$A = 1 + 2 \frac{\Delta_m}{\Delta_{31}} (1 - 2s_{13}^2) - \Delta_{21} \frac{j}{l} \sin \delta - \Delta_{21} \frac{\Delta_m j}{\Delta_{31} l} \left(\sin \delta + \frac{\Delta_{31}}{2} \cos \delta \right) + \frac{\Delta_{21}^2 j}{2} \frac{j}{l} \left[\frac{j}{l} \cos \delta + (1 - 2s_{12}^2) \right] \cos \delta + 3 \frac{\Delta_m^2}{\Delta_{31}^2}, \quad (4.1b)$$

$$\Theta = \frac{\Delta_{31}}{2} - \frac{\Delta_m}{2} (1 - 2s_{13}^2) + \frac{\Delta_{21}}{2} \left(\frac{j}{l} \cos \delta - s_{12}^2 \right) - \frac{\Delta_{21}}{2} \frac{\Delta_m j}{\Delta_{31} l} \left(\cos \delta + \frac{\Delta_{31}}{2} \sin \delta \right) + \frac{\Delta_{21}^2 j}{2} \frac{j}{l} \left[\frac{j}{l} \cos \delta + \frac{1}{2} (1 - 2s_{12}^2) \right] \sin \delta, \quad (4.1c)$$

and

$$B = \frac{\Delta_{21}^2 j^2}{4 l^2} \sin^2 \delta. \quad (4.1d)$$

Here $\Delta_{ij} = \delta m_{ij}^2 L/2E$, $l = c_{13}^2 s_{13}^2 s_{23}^2$, and $j = c_{13}^2 s_{13} c_{23} s_{23} c_{12} s_{12}$, where $s_{ij} = \sin \theta_{ij}$, and $c_{ij} = \cos \theta_{ij}$. The approximation we employed in deriving Eq. (4.1) is suitable especially for a short baseline, typically for $L < O(10^3 \text{ km})$; see Appendix B. The oscillation probability for anti-neutrinos $P(\bar{\nu}_\mu \rightarrow \bar{\nu}_e, E)$ is obtained by changing the signs of δ and Δ_m .

We obtain the peak energy, which gives the local maxima of the oscillation probability of Eq. (4.1), as

$$\begin{aligned} E_{\text{peak},n} = \frac{|\delta m_{31}^2| L}{2\Pi} & \left\{ \left[1 \mp \Delta_m \frac{1}{\Pi} \left(1 - \frac{4}{\Pi^2} \right) (1 - 2s_{13}^2) \right. \right. \\ & \mp R s_{12}^2 + \Delta_m^2 \frac{1}{\Pi^2} \left(1 - \frac{12}{\Pi^2} + \frac{48}{\Pi^4} \right) - R^2 \frac{1}{2} \left(1 - \frac{4}{\Pi^2} \right) \frac{j^2}{l^2} \left. \right] \\ & + R \left[\pm 1 - \Delta_m \frac{1}{\Pi} \left(1 - \frac{8}{\Pi^2} \right) - 2R(1 - 2s_{12}^2) \right] \frac{j}{l} \cos \delta \\ & + R \frac{2}{\Pi} \left[1 \mp \Delta_m \frac{\Pi}{4} \left(1 + \frac{8}{\Pi^2} - \frac{64}{\Pi^4} \right) \pm R \frac{\Pi^2}{4} (1 - 2s_{12}^2) \right] \frac{j}{l} \sin \delta \\ & \left. - R^2 \frac{3}{2} \left(1 + \frac{4}{3} \frac{1}{\Pi^2} \right) \frac{j^2}{l^2} \cos 2\delta \pm R^2 \frac{\Pi}{2} \frac{j^2}{l^2} \sin 2\delta \right\}, \end{aligned} \quad (4.2)$$

where $n = 0, 1, 2, \dots$ is the peak index, $\Pi \equiv (2n + 1)\pi$, $R \equiv \delta m_{21}^2 / |\delta m_{31}^2|$, and the top of the double sign is for $\delta m_{31}^2 > 0$ and the bottom for $\delta m_{31}^2 < 0$. The oscillation probability at the peak energy is given by

$$\begin{aligned} P_{\text{peak},n} = 4l & \left\{ \left[1 \pm \Delta_m \frac{2}{\Pi} (1 - 2s_{13}^2) + R^2 \frac{3}{8} \Pi^2 \left(1 + \frac{4}{3} \frac{1}{\Pi^2} \right) \frac{j^2}{l^2} \right. \right. \\ & + \Delta_m^2 \frac{1}{\Pi^2} \left(1 + \frac{4}{\Pi^2} \right) \left. \right] - R \frac{\Pi^2}{2} \left[\Delta_m \frac{1}{\Pi} \left(1 - \frac{4}{\Pi^2} \right) - R(1 - 2s_{12}^2) \right] \frac{j}{l} \cos \delta \\ & - R\Pi \left[1 \pm \Delta_m \frac{2}{\Pi} \left(1 - \frac{2}{\Pi^2} \right) \pm R s_{12}^2 \right] \frac{j}{l} \sin \delta \\ & \left. + R^2 \frac{\Pi^2}{8} \left(1 - \frac{4}{\Pi^2} \right) \frac{j^2}{l^2} \cos 2\delta \pm R^2 \frac{\Pi}{2} \frac{j^2}{l^2} \sin 2\delta \right\}. \end{aligned} \quad (4.3)$$

A peak loop is obtained when we keep track of $(E_{\text{peak},n}, P_{\text{peak},n})$ as we vary δ with other parameters fixed. We present in Fig. 6 the peak loops for the first peak ($n = 0$) obtained from Eqs. (4.2) and (4.3) and compare them with the numerical results to confirm good agreement.

The basic properties of the peak loop are its position, size, and shape, and we quantify them using its central position, width, and height, respectively, as follows.

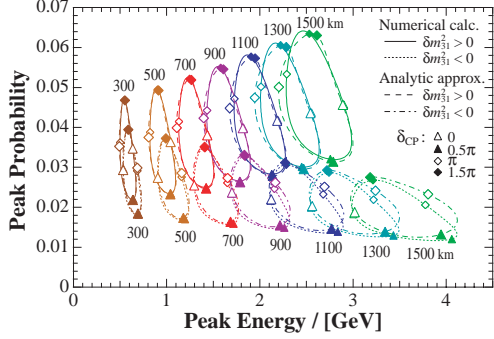


Fig. 6. Trajectories of the first oscillation peak for baseline lengths between 300 km and 1500 km obtained from the numerical calculation (the solid curve for the normal hierarchy and the dotted for the inverted) and analytic approximations (the dashed curve for the normal hierarchy and the dash-dotted for the inverted). The oscillation parameters in Eq. (2·1) are adopted.

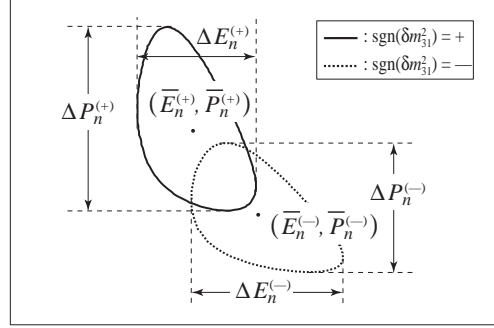


Fig. 7. Notations to designate the central position, the width, and the height of the trajectories of the $(n + 1)$ -th oscillation peak.

The terms independent of δ in the braces of Eqs. (4·2) and (4·3) give the average values of $E_{\text{peak},n}$ and $P_{\text{peak},n}$ over a cycle of δ and can be regarded as the center of a peak loop. The central position up to first order thus reads

$$\begin{aligned} (\bar{E}_n^{(\pm)}, \bar{P}_n^{(\pm)}) = & \left(\frac{|\delta m_{31}^2| L}{2\Pi} \left[1 \mp \Delta_m \frac{1}{\Pi} \left(1 - \frac{4}{\Pi^2} \right) (1 - 2s_{13}^2) \mp R s_{12}^2 \right], \right. \\ & \left. 4l \left[1 \pm \Delta_m \frac{2}{\Pi} (1 - 2s_{13}^2) \right] \right), \end{aligned} \quad (4·4)$$

where the double sign is the same as in Eqs. (4·2) and (4·3); see Fig. 7. The terms that depend on δ in Eqs. (4·2) and (4·3) account for the size and the shape of a peak loop. The width of a loop $\Delta E_n^{(\pm)}$ and its height $\Delta P_n^{(\pm)}$ can be estimated by taking the difference of the maximum and minimum values of $E_{\text{peak},n}$ and $P_{\text{peak},n}$ as functions of δ (see Fig. 7). They are calculated up to second order as

$$\begin{aligned} \Delta E_n^{(\pm)} = & |\delta m_{31}^2| L R \frac{1}{\Pi} \sqrt{1 + \frac{4}{\Pi^2} \frac{j}{l}} \\ & \times \left[1 \mp \Delta_m \frac{2}{\Pi} \frac{1 - 32/\Pi^4}{1 + 4/\Pi^2} \mp R \frac{1}{1 + 4/\Pi^2} (1 - 2s_{12}^2) \right], \end{aligned} \quad (4·5a)$$

$$\Delta P_n^{(\pm)} = 8R\Pi j \left[1 \pm \Delta_m \frac{2}{\Pi} \left(1 - \frac{2}{\Pi^2} \right) \pm R s_{12}^2 \right]. \quad (4·5b)$$

We remark on the magnitude of the correction terms appearing in Eqs. (4·4) and (4·5). The correction terms include the matter effect proportional to Δ_m and

the three-generation effect proportional to R . Of these two, the three-generation effect is even smaller than the matter effect for a typical long baseline experiments. Evaluation using the example values given in Eq. (2.1) is sufficient to verify this with an order-of-magnitude estimation, which yields

$$\Delta_m \frac{1}{\Pi} \sim 0.2 \left(\frac{L}{1000 [\text{km}]} \right) \quad \text{for } n = 0, \quad R(1 - 2s_{12}^2) \sim Rs_{12}^2 \sim 0.01. \quad (4.6)$$

The expressions for anti-neutrinos are obtained from Eqs. (4.4) and (4.5) by simply flipping the signs of Δ_m :

$$\begin{aligned} (\overline{E}_n^{(\pm)}, \overline{P}_n^{(\pm)}) = & \left(\frac{|\delta m_{31}^2| L}{2\Pi} \left[1 \pm \Delta_m \frac{1}{\Pi} \left(1 - \frac{4}{\Pi^2} \right) (1 - 2s_{13}^2) \mp Rs_{12}^2 \right], \right. \\ & \left. 4l \left[1 \mp \Delta_m \frac{2}{\Pi} (1 - 2s_{13}^2) \right] \right), \end{aligned} \quad (4.7)$$

$$\begin{aligned} \Delta E_n^{(\pm)} = & |\delta m_{31}^2| LR \frac{1}{\Pi} \sqrt{1 + \frac{4}{\Pi^2} \frac{j}{l}} \\ & \times \left[1 \pm \Delta_m \frac{2}{\Pi} \frac{1 - 32/\Pi^4}{1 + 4/\Pi^2} \mp R \frac{1}{1 + 4/\Pi^2} (1 - 2s_{12}^2) \right], \end{aligned} \quad (4.8a)$$

$$\Delta P_n^{(\pm)} = 8R\Pi j \left[1 \mp \Delta_m \frac{2}{\Pi} \left(1 - \frac{2}{\Pi^2} \right) \pm Rs_{12}^2 \right]. \quad (4.8b)$$

Equations (4.7) and (4.8) have an interesting relation to (4.4) and (4.5). The former pair for anti-neutrinos is equivalent to the latter for neutrinos with flipped hierarchy up to the correction terms proportional to Rs_{12}^2 or $R(1 - 2s_{12}^2)$, which are small as shown in Eq. (4.6).

4.2. Analysis of the peak loops

We elevate the observation of peak loops for neutrinos shown by Fig. 5 to a systematic analysis by applying the formulae we developed in the previous subsection. We also extend our consideration to the anti-neutrino case.

Equation (4.4) reveals the order behind the motion of the loops for neutrinos in the E - P plane as the baseline length becomes longer. The leading dependence of $\overline{E}_n^{(\pm)}$ on the baseline length comes from the prefactor $|\delta m_{31}^2| L/2E$ and drives the loops rightward. Its subleading dependence due to the matter-effect term, which is proportional to the baseline length through Δ_m and to $\text{sgn } \delta m_{31}^2$, provides a correction which pulls the normal loop back leftward and gives the inverted loop another push rightward. The other subleading term Rs_{12}^2 of $\overline{E}_n^{(\pm)}$ gives an extra correction whose sign depends on the hierarchy and whose magnitude depends on the mass parameters and the mixing parameters but not on the baseline length. The dependence of $\overline{P}_n^{(\pm)}$ on the baseline length comes from the matter-effect term, which raises the normal loop and lowers the inverted loop. As a whole, a pair of normal and inverted loops are driven rightward while they split vertically, and their alignment

tilts counterclockwise. These features of the motion of the loops are clearly observed in Fig. 5.

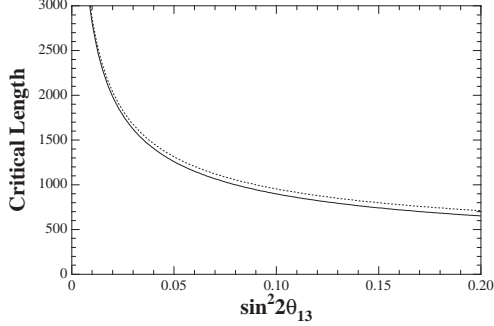


Fig. 8. The critical length as a function of $\sin^2 2\theta_{13}$ in the first-order approximation, Eq. (4.9). The solid curve is for neutrinos and the dotted curve for anti-neutrinos. We adopt the values of the oscillation parameters given in Eq. (2.1) except for that of $\sin^2 2\theta_{13}$ in Eq. (2.1e).

term, which vertically stretches the normal loop and compresses the inverted loop, and the other correction term supplements its effect. All these features of the loops are evident in Fig. 5.

Now that the motion and the distortion of the loops for the neutrinos have been analyzed, those for anti-neutrinos are easy to derive owing to the discussion below Eq. (4.8) in the previous subsection. A loop for anti-neutrinos moves with distortion just as that for neutrinos with the opposite hierarchy, except for the small contribution of the three-generation effect.

The critical baseline length mentioned in the previous section also can be analyzed with our formulation. The critical length is defined as the maximum length giving the intersection of the pairing loops with opposite hierarchies. It is calculated in the first-order approximation as

$$L_{\text{crit}} = \frac{1}{\sqrt{2}G_F n_e} \frac{\Pi}{1 - \frac{12}{\Pi^2} + \frac{64}{\Pi^4}} R \frac{c_{23}c_{12}s_{12}}{s_{13}s_{23}} \frac{1}{1 - 2s_{13}^2} \times \left[\sqrt{1 - \frac{12}{\Pi^2} + \frac{64}{\Pi^4} - \frac{4}{\Pi^2} \left(\frac{s_{13}s_{23}s_{12}}{c_{23}c_{12}} \right)^2} \mp \left(1 - \frac{8}{\Pi^2} \right) \frac{s_{13}s_{23}s_{12}}{c_{23}c_{12}} \right], \quad (4.9)$$

where the double sign is $-$ for neutrinos and $+$ for anti-neutrinos. The prefactor appearing on the right-hand side of this expression gives $1/\sqrt{2}G_F n_e = 5.17 \times 10^3 \text{ [km]} \times (\rho/[\text{g cm}^{-3}])^{-1} = 2.0 \times 10^3 \text{ [km]} \cdot (\rho/[2.6 \text{ g cm}^{-3}])^{-1}$. The critical length is inversely proportional to $\sin \theta_{13}$ owing to the factor $c_{23}c_{12}s_{12}/s_{13}s_{23}$, with the small correction of $O(\theta_{13})$. It is particularly important that this dependence can make the critical length very long, since the lower bound on the value of $\sin \theta_{13}$ is unknown at present.

We next analyze the distortion of the loop for neutrinos in terms of its width and height given in Eq. (4.5). The expression for $\Delta E_n^{(\pm)}$ has an overall factor which is proportional to the baseline length and accounts for the widening of the loops. One of two subleading corrections of $\Delta E_n^{(\pm)}$ is the matter-effect term, which adds a dependence on the baseline length. The other term also gives a correction, but does not give any additional dependence on the baseline length. Both of these terms depend on the hierarchy, and decelerate the widening of the normal loop and accelerate that of the inverted loop. The dependence of $\Delta P_n^{(\pm)}$ on the baseline length is due to the subleading matter-effect

Figure 8 shows the dependence of the critical length on $\sin^2 2\theta_{13}$ for the first peak, where the other parameters are fixed to the values given in Eq. (2.1). The critical length for anti-neutrinos is slightly longer than that for neutrinos due to the small correction proportional to $s_{13}s_{23}s_{12}/c_{23}c_{12}$. From this graph, we find $L_{\text{crit}} = 1150$ km for neutrinos and $L_{\text{crit}} = 1200$ km for anti-neutrinos at $\sin^2 2\theta_{13} = 0.06$. This graph is qualitatively consistent with Fig. 5 in Ref. 16), which is obtained from their bi-channel analysis with the energy fixed around a peak at $E = |\delta m_{31}^2|L/2\pi$.

It is remarkable that the following straightforward analysis of the loops reproduces the main part of Eq. (4.9), which is tedious to derive, and clarifies the origin of the dependence of the critical length upon the mass parameters and the mixing parameters. We compare the separation between the loops with their size to obtain a condition for their disentanglement. The separation of the two loops is estimated using the difference between the respective values of $\overline{E}^{(\pm)}$ and $\overline{P}^{(\pm)}$, while the size of each loop is measured by its width and height. We consider the ratio of the separation to the size to compare the two, and define a normalized separation vector as

$$\begin{aligned} & \left(\frac{\overline{E}_n^{(+)} - \overline{E}_n^{(-)}}{[\Delta E_n^{(+)} + \Delta E_n^{(-)}]/2}, \frac{\overline{P}_n^{(+)} - \overline{P}_n^{(-)}}{[\Delta P_n^{(+)} + \Delta P_n^{(-)}]/2} \right) \\ & \simeq \frac{\Delta_m}{R} \frac{l}{j} (1 - 2s_{13}^2) \left(-\frac{1}{\Pi} \frac{1 - 4/\Pi^2}{\sqrt{1 + 4/\Pi^2}}, \frac{2}{\Pi^2} \right), \end{aligned} \quad (4.10)$$

where we have omitted small terms such as Rs_{12}^2 and $R(1 - s_{12}^2)$ on the right-hand side for simplicity. The magnitude of this vector is given by

$$S(L) \simeq \frac{\Delta_m}{R} \frac{l}{j} (1 - 2s_{13}^2) \frac{1}{\Pi} = \frac{\sqrt{2}G_F n_e}{(2n + 1)\pi} L \frac{1}{R} \frac{l}{j} (1 - 2s_{13}^2), \quad (4.11)$$

which is proportional to L and parametrizes the configuration of the paired loops, *i.e.* intersected, tangential, or disjoint. The normalization of Eq. (4.10) is chosen so that the separation at the critical length $S_{\text{crit}} \equiv S(L_{\text{crit}})$ becomes unity when the loops are two similar ellipses whose major axes are parallel. We write the critical length from Eq. (4.11) as

$$L_{\text{crit}} = \frac{(2n + 1)\pi}{\sqrt{2}G_F n_e} R \frac{c_{23}c_{12}s_{12}}{s_{23}} \frac{1}{s_{13}} \frac{1}{1 - 2s_{13}^2} S_{\text{crit}}. \quad (4.12)$$

Equation (4.12) approximately reproduces the dependence on the parameters appearing on the right-hand side of Eq. (4.9), assuming that S_{crit} does not give any extra dependence on the mass parameters and the mixing parameters.

§5. Toward a resolution of the hierarchy degeneracy

In this section, we consider how to avoid the hierarchy degeneracy in determining the value of δ with long baseline experiments.

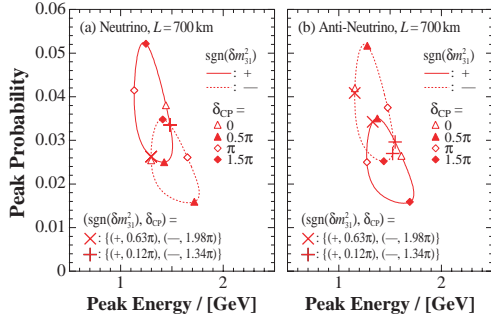


Fig. 9. Trajectories of the first peak of (a) the $\nu_\mu \rightarrow \nu_e$ probability and (b) the $\bar{\nu}_\mu \rightarrow \bar{\nu}_e$ probability for a baseline length of 700 km. The solid and dotted curves are for the normal and inverted hierarchies, respectively. The “x” and “+” symbols in (a) are on the intersections of the peak loops, and the corresponding values of the parameters are also shown. The symbols in (b) mark the points corresponding to these parameter values.

problem, we can simultaneously make use of two or more peaks. We examine the effectiveness of the following three approaches of this kind: (2) observing $\bar{\nu}_\mu \rightarrow \bar{\nu}_e$ appearance events in addition to $\nu_\mu \rightarrow \nu_e$ events; (3) carrying out two or more experiments with different baseline lengths; and (4) carrying out an experiment which has two or more oscillation peaks within its range of visible neutrino energy.

The second approach employs both neutrinos and anti-neutrinos. We analyze the merit of this approach with Fig. 9, which presents two pairs of peak loops, one (a) for neutrinos and the other (b) for anti-neutrinos, with the values of Eq. (2-1) and $L = 700$ km. The loops in Figs. 9(a) and (b) resemble each other with opposite assignments of the hierarchy, confirming our discussion in §4.2 based on analytic formulae. Marked by the “x” and “+” symbols in Fig. 9(a) are the two intersections of the normal and inverted loops. Each intersection is associated with two sets of $(\text{sgn } \delta m_{31}^2, \delta)$ as we gave examples in Eq. (3-1) and corresponds to the presence of the hierarchy degeneracy. Turning to Fig. 9(b), the four parameter sets considered there correspond to four distinct points on the peak loops for anti-neutrinos. Hence the combined analysis of $\nu_\mu \rightarrow \nu_e$ events and $\bar{\nu}_\mu \rightarrow \bar{\nu}_e$ events will be able to resolve the hierarchy degeneracy, provided that the two “x” symbols or the two “+” symbols are experimentally distinguishable. In our present example, the two “+” symbols for anti-neutrinos are close to each other in the E - P plane and are thus difficult to distinguish. If indistinguishable, the hierarchy degeneracy will persist even with the aid of anti-neutrino events.

The third approach makes use of two or more different baseline lengths.¹⁵⁾ We reproduce in Fig. 10 the series of peak loops shown in Fig. 5. On top of them, we mark the points corresponding to the parameter values for the intersections of the loops in the case $L = 700$ km as we did in Fig. 9. Each pair of loops for a

A promising approach for determining the value of δ and the hierarchy is (1) to carry out an experiment with baseline length longer than the critical length so that the hierarchy is identified regardless of the value of δ . This approach can be made feasible by pinning down the position of only one peak. It is nonetheless not free of hurdles: the required baseline length is typically about 1000 km and may be even longer, depending on the value of θ_{13} . Performing experiments with such a long baseline is challenging due to, for instance, the small flux of the neutrino beam and a possible large ambiguity of matter effects.

Experiments with shorter baselines are more feasible, but leave the possibility of degeneracy. To overcome this

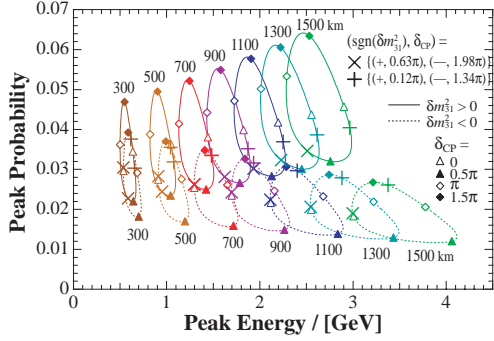


Fig. 10. The positions of the first peak for baseline lengths between 300 km and 1500 km. The “x” and “+” symbols indicate the positions for the four sets of parameter values which correspond to the two intersections of the peak loops at $L = 700$ km, and they are plotted on top of the series of peak loops reproduced from Fig. 5. The parameter values given in Eq. (2.1) are adopted. The solid (dotted) curve is for the normal (inverted) hierarchy.

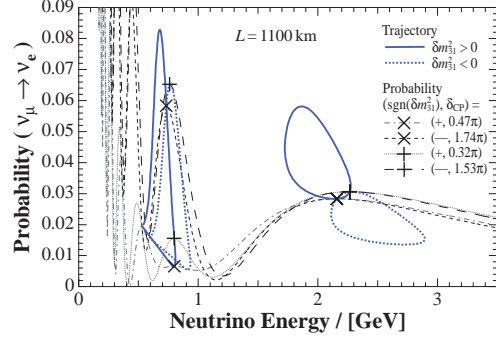


Fig. 11. Trajectories of the first and second oscillation peaks for $L = 1100$ km. The parameter values given in Eq. (2.1) are adopted. The solid (dotted) loop is for the normal (inverted) hierarchy. The “x” and “+” symbols correspond to the sets of parameter values for which the first peak is at the intersection of its trajectories. The points for these values are also on the second peak loops and are marked by the corresponding symbols. The oscillation spectra for the parameter values are overlaid.

fixed baseline length has two “x” symbols and two “+” symbols, which reduce, by definition, to a single “x” symbol and a single “+” symbol at $L = 700$ km. The separation between the two “x” symbols as well as between the two “+” symbols grows as the baseline length deviates from 700 km. The degeneracy of the two “x” symbols or the two “+” symbols can thus be resolved with an additional experiment with a different baseline length, where the large difference between the two baseline lengths is preferable.

The fourth approach exploits other peaks of the appearance probability in addition to the first one for $n = 0$.²⁰⁾ This approach requires a wide-band neutrino beam in order to accumulate a sufficient number of events at the multiple peaks. An analysis covering peaks for different values of n is effective to resolve the degeneracy since each peak has its own properties due to the factor $\Pi \equiv (2n + 1)\pi$ in Eqs. (4.4) and (4.5). The peak for $n > 0$, however, is not easy to observe due to its small energy which is suppressed by the factor of $1/(2n + 1)$. On the other hand, elongation of the baseline makes the peak energies higher, bringing both the first and second peaks within the range of visible energy. We show in Fig. 11 the two sets of loops traced by the first and second peaks for $L = 1100$ km. The second-peak loops are stretched in the P -direction and have a significant overlap, showing their noticeable difference from the first-peak loops. The “x” and “+” symbols correspond to the values at the two intersections of the loops for the first peak. On the second peak loops, the paired “x” symbols as well as the paired “+” symbol are separated from each other and are experimentally distinguishable. The hierarchy degeneracy in the first peak will be thereby removed by observing the second peak.

§6. Conclusion and discussion

We have studied the search for the leptonic CP -violating phase δ and the neutrino mass hierarchy $\text{sgn} \delta m_{31}^2$ through the observation of the $\nu_\mu \rightarrow \nu_e$ oscillation with long baseline experiments. The energy spectrum of the $\nu_\mu \rightarrow \nu_e$ appearance probability is engraved with the values of these parameters, although not uniquely. The search for these parameters through this spectrum can lead to degeneracy when the two spectra corresponding to the two different parameter values are indistinguishable. We implemented the presence of degeneracy using the following criterion: the oscillation probabilities for the two parameter values are peaked at the same energy and have the same peak probability. In light of this peak-matching condition, we systematically examined the presence and absence of degeneracy, especially the hierarchy degeneracy with regard to the value of δ and the sign of δm_{31}^2 . We have also demonstrated the prospects for resolving the degeneracy using a single experiment and combinations of experiments.

We introduced a looped trajectory traced by the position of the oscillation peak in the E - P plane while varying the value of δ over the interval $[0, 2\pi]$. We have shown that the loop plays a key rôle in gaining an intuitive understanding of the parameter degeneracy. We drew pairs of loops for both hierarchies and investigated their properties and behavior to obtain an overview of the emergence of the hierarchy degeneracy and methods to avoid it. We observed that paired loops with different hierarchies are completely separated when the baseline is longer than a critical length, which is proportional to $1/\sin \theta_{13}$ and is typically about 1000 km or longer. The hierarchy degeneracy can be avoided in experiments with a baseline length longer than the critical length.

Employing the peak loops, we obtained a general understanding of experimental capabilities to determine the value of δ and the mass hierarchy. We described four ideas for resolving degeneracy with long baseline experiments: using a baseline longer than the critical length, employing anti-neutrinos as well as neutrinos, using two or more different baseline lengths, and carrying out experiments covering two or more oscillation peaks. We discussed the merits and demerits of each idea in terms of the peak loops. We pointed out that the first idea of using a sufficiently long baseline is simple but is not free of hurdles. We also found for the second case that employing anti-neutrinos does not always resolve the hierarchy degeneracy.

The peak loops we introduced to analyze the parameter degeneracy is as versatile as the trajectories in the bi-channel plots presented in Ref. 12). The two have differences at the same time. One difference is that our plot employs only a single channel and thus can be used to explore the capabilities of single-channel experiments. Another difference is that we make essential use of the oscillation peak as a representative of the oscillation spectrum over a finite energy range, while the bi-channel plot is drawn for an arbitrary fixed energy or for integrated values over an energy range at one's convenience. The significance of the peak position consists in its implication to the values of the parameters for which we search. Supported by the peak-matching condition, our method facilitates a direct prediction of the presence of degeneracy.

We kept the values of the mass parameters and the mixing parameters fixed except for δ and $\text{sgn } \delta m_{31}^2$, assuming that their values will be determined before the experiments in question are carried out. It is possible, however, that they will not be determined with sufficient precision by that time and that their ambiguities will add another complication to the searches.^{9),10)} The peak loops presented in this paper also offer an intuitive understanding of the effects of these ambiguities. The position of the oscillation peak moves around in the E - P plane when the value of a parameter is ambiguous and varies within its allowed region. The peak position will thus be smeared and consequently the loop of the peak will appear broadened and blurred. The value of δ will be accordingly obscured and the mass hierarchy will be misidentified within the extended region around the intersection of the loops. In addition, the broadening of a narrow loop makes its parallel sides indistinguishable. We hence expect that ambiguities of the mass parameters and the mixing parameters will worsen the degeneracy of the target parameters and hinder attempts to determine them. We need extra effort to keep the ambiguities under control, such as combining with the $\nu_\mu \rightarrow \nu_\mu$ disappearance channel or employing reactor neutrino experiments. Detailed analyses of the ambiguities in the framework of the peak loops are left for future works.

The present analysis based on the peak loops for the oscillation probability is independent of experimental specifications and gives an organized understanding of the presence and absence of degeneracy. A more practical evaluation of quantitative capabilities can be carried out for specific experiments by applying the expected number of events to our analysis in place of the oscillation probability. For that purpose, we need to calculate the expected number of events by using the neutrino beam flux of the experiment, the neutrino cross sections, the detector design including a knowledge of systematic errors and background, and other aspects of the experimental setup. Drawing the loops traced by the peaks of the spectrum of the event number, we can study the possibility of the presence of degeneracy, quantitatively estimate the allowed region in the parameter space, and select an appropriate baseline length to determine the parameter values.

Acknowledgements

The authors are grateful to Professor Joe Sato for his encouragement during this work.

Appendix A

— Oscillation Probabilities to Second Order —

We calculate the S -matrix of neutrino oscillation to second order in $\Delta_{21} \equiv \delta m_{21}^2 L/2E$ and $\Delta_m = aL/2E$, and also derive a formula for the oscillation probability to this order.

The evolution equation of neutrinos $\nu = (\nu_e, \nu_\mu, \nu_\tau)^T$ is given by

$$i \frac{d\nu(x)}{dx} = H(x)\nu(x), \quad (\text{A}\cdot 1)$$

where

$$H(x) = \frac{1}{2E} \left(U \text{diag}(0, \delta m_{21}^2, \delta m_{31}^2) U^\dagger + \text{diag}(a(x), 0, 0) \right). \quad (\text{A}\cdot 2)$$

Here E is the neutrino energy, U is the unitary mixing matrix of the neutrinos (MNS matrix), and $a(x) = 2\sqrt{2}G_{\text{F}}n_e(x)E$ represents the matter effect, where G_{F} is the Fermi constant and $n_e(x)$ is the number density of electrons on the baseline. The probability for a neutrino ν_α to change into ν_β ($\{\alpha, \beta\} \subset \{e, \mu, \tau\}$) is given by

$$P(\nu_\alpha \rightarrow \nu_\beta) = |S(x)_{\beta\alpha}|^2, \quad (\text{A}\cdot 3)$$

where

$$S(x) = \text{T exp} \left(-i \int_0^x ds H(s) \right). \quad (\text{A}\cdot 4)$$

We assume in this paper that the spatial variation of the electron density n_e is negligible so that Eq. (A·4) simplifies to

$$S(x) = e^{-iHx}. \quad (\text{A}\cdot 5)$$

We split H as $H = H_0 + H_1$, where we have

$$H_0 \equiv \frac{1}{2E} U \text{diag}(0, 0, \delta m_{31}^2) U^\dagger, \quad (\text{A}\cdot 6)$$

$$H_1 \equiv \frac{1}{2E} \left(U \text{diag}(0, \delta m_{21}^2, 0) U^\dagger + \text{diag}(a, 0, 0) \right), \quad (\text{A}\cdot 7)$$

and treat H_1 as a perturbation to obtain

$$S(x) = e^{-iH_0x} \text{T exp} \left(-i \int_0^x ds e^{iH_0s} H_1 e^{-iH_0s} \right). \quad (\text{A}\cdot 8)$$

Expansion of Eq. (A·8) leads to a systematic approximation of S -matrix.²¹⁾ An explicit calculation of $S(x)$ up to the second order in H_1 gives

$$S(x)_{\beta\alpha} = S_0(x)_{\beta\alpha} + S_1(x)_{\beta\alpha} + S_2(x)_{\beta\alpha}, \quad (\text{A}\cdot 9)$$

where

$$S_0(x)_{\beta\alpha} = \delta_{\alpha\beta} - U_{\beta 3} U_{\alpha 3}^* (1 - e^{-i\Delta_{31}}), \quad (\text{A}\cdot 10)$$

$$\begin{aligned} S_1(x)_{\beta\alpha} = & -i\Delta_{21} U_{\beta 2} U_{\alpha 2}^* \\ & -i\Delta_{\text{m}} \left[\delta_{\beta e} \delta_{\alpha e} - (\delta_{\alpha e} + \delta_{\beta e}) U_{\beta 3} U_{\alpha 3}^* + |U_{e3}|^2 U_{\beta 3} U_{\alpha 3}^* (1 + e^{-i\Delta_{31}}) \right] \\ & - \frac{\Delta_{\text{m}}}{\Delta_{31}} (\delta_{\alpha e} + \delta_{\beta e} - 2|U_{e3}|^2) U_{\beta 3} U_{\alpha 3}^* (1 - e^{-i\Delta_{31}}), \end{aligned} \quad (\text{A}\cdot 11)$$

and

$$\begin{aligned}
 S_2(x)_{\beta\alpha} = & -\frac{1}{2}\Delta_{21}^2 U_{\beta 2} U_{\alpha 2}^* \\
 & - \Delta_m \Delta_{21} \left[\frac{1}{2}(\delta_{\alpha e} + \delta_{\beta e}) U_{\beta 2} U_{\alpha 2}^* \right. \\
 & \quad \left. - (U_{e2} U_{e3}^* U_{\beta 3} U_{\alpha 2}^* + U_{e3} U_{e2}^* U_{\beta 2} U_{\alpha 3}^*) \left(\frac{1}{2} + \frac{i}{\Delta_{31}} - \frac{1 - e^{-i\Delta_{31}}}{\Delta_{31}^2} \right) \right] \\
 & - \Delta_m^2 \left(\frac{1}{2} \delta_{\beta e} \delta_{\alpha e} - (\delta_{\alpha e} + \delta_{\beta e}) U_{\beta 3} U_{\alpha 3}^* \left(\frac{1}{2} + \frac{i}{\Delta_{31}} - \frac{1 - e^{-i\Delta_{31}}}{\Delta_{31}^2} \right) \right. \\
 & \quad \left. + |U_{e3}|^2 \left\{ -\delta_{\beta e} \delta_{\alpha e} \left(\frac{1}{2} + \frac{i}{\Delta_{31}} - \frac{1 - e^{-i\Delta_{31}}}{\Delta_{31}^2} \right) \right. \right. \\
 & \quad \left. \left. + (1 + \delta_{\alpha e} + \delta_{\beta e}) U_{\beta 3} U_{\alpha 3}^* \left[\frac{1}{2} + \frac{i(2 + e^{-i\Delta_{31}})}{\Delta_{31}} - \frac{3(1 - e^{-i\Delta_{31}})}{\Delta_{31}^2} \right] \right\} \right. \\
 & \quad \left. - |U_{e3}|^4 U_{\beta 3} U_{\alpha 3}^* \left[\frac{1 - e^{-i\Delta_{31}}}{2} + \frac{3i(1 + e^{-i\Delta_{31}})}{\Delta_{31}} - \frac{6(1 - e^{-i\Delta_{31}})}{\Delta_{31}^2} \right] \right), \tag{A.12}
 \end{aligned}$$

with $\Delta_{ij} \equiv \delta m_{ij}^2 L/2E$ and $\Delta_m \equiv aL/2E$. Substituting Eqs. (A.10), (A.11) and (A.12) into Eq. (A.3), we obtain the expression for the oscillation probability up to second order as

$$P(\nu_\alpha \rightarrow \nu_\beta) = p_0(\nu_\alpha \rightarrow \nu_\beta) + p_1(\nu_\alpha \rightarrow \nu_\beta) + p_2(\nu_\alpha \rightarrow \nu_\beta), \tag{A.13a}$$

where

$$p_0(\nu_\alpha \rightarrow \nu_\beta) = \delta_{\alpha\beta} - 4|U_{\beta 3}|^2 (\delta_{\alpha\beta} - |U_{\alpha 3}|^2) s^2, \tag{A.13b}$$

$$\begin{aligned}
 p_1(\nu_\alpha \rightarrow \nu_\beta) = & 4\Delta_{21} \left[\text{Re} (U_{\beta 3}^* U_{\beta 2} U_{\alpha 3} U_{\alpha 2}^*) sc - \text{Im} (U_{\beta 3}^* U_{\beta 2} U_{\alpha 3} U_{\alpha 2}^*) s^2 \right] \\
 & + 4\Delta_m |U_{e3}|^2 (\delta_{\alpha e} \delta_{\beta e} - \delta_{\alpha e} |U_{\beta 3}|^2 - \delta_{\beta e} |U_{\alpha 3}|^2 \\
 & \quad - \delta_{\alpha\beta} |U_{\beta 3}|^2 + 2|U_{\beta 3}|^2 |U_{\alpha 3}|^2) \left(sc - \frac{2}{\Delta_{31}} s^2 \right), \tag{A.13c}
 \end{aligned}$$

and

$$p_2(\nu_\alpha \rightarrow \nu_\beta) = \Delta_{21}^2 p_{2A} + \Delta_{21} \Delta_m p_{2B} + \Delta_m^2 p_{2C}, \tag{A.13d}$$

with

$$\begin{aligned}
 p_{2A} = & -(\delta_{\alpha\beta} - |U_{\alpha 2}|^2) |U_{\beta 2}|^2 + 2 \text{Re} (U_{\beta 3}^* U_{\beta 2} U_{\alpha 3} U_{\alpha 2}^*) s^2 \\
 & + 2 \text{Im} (U_{\beta 3}^* U_{\beta 2} U_{\alpha 3} U_{\alpha 2}^*) sc, \tag{A.13e}
 \end{aligned}$$

$$\begin{aligned}
p_{2B} = & -2(\delta_{\alpha e} + \delta_{\beta e} - 2|U_{e3}|^2) \operatorname{Re}(U_{\beta 3}^* U_{\beta 2} U_{\alpha 3} U_{\alpha 2}^*) \left(1 - s^2 - \frac{2}{\Delta_{31}} sc\right) \\
& + 2\delta_{\alpha\beta} \operatorname{Re}(U_{\beta 3}^* U_{\beta 2} U_{e3} U_{e2}^*) \left(1 - \frac{4}{\Delta_{31}^2} s^2\right) \\
& - 2 \left[|U_{\beta 3}|^2 \operatorname{Re}(U_{e3}^* U_{e2} U_{\alpha 3} U_{\alpha 2}^*) + |U_{\alpha 3}|^2 \operatorname{Re}(U_{\beta 3}^* U_{\beta 2} U_{e3} U_{e2}^*) \right] \\
& \quad \times \left(s^2 + \frac{2}{\Delta_{31}} sc - \frac{4}{\Delta_{31}^2} s^2 \right) \\
& - 2 \left[|U_{\beta 3}|^2 \operatorname{Im}(U_{e3}^* U_{e2} U_{\alpha 3} U_{\alpha 2}^*) + |U_{\alpha 3}|^2 \operatorname{Im}(U_{\beta 3}^* U_{\beta 2} U_{e3} U_{e2}^*) \right. \\
& \quad \left. - (\delta_{\alpha e} + \delta_{\beta e} - 2|U_{e3}|^2) \operatorname{Im}(U_{\beta 3}^* U_{\beta 2} U_{\alpha 3} U_{\alpha 2}^*) \right] \left(sc - \frac{2}{\Delta_{31}} s^2 \right),
\end{aligned} \tag{A.13f}$$

and

$$\begin{aligned}
p_{2C} = & -|U_{e3}|^2 (\delta_{\alpha e} \delta_{\beta e} - \delta_{\alpha e} |U_{\beta 3}|^2 - \delta_{\beta e} |U_{\alpha 3}|^2) \left(1 - 2s^2 - \frac{8}{\Delta_{31}} sc + \frac{12}{\Delta_{31}^2} s^2\right) \\
& - \delta_{\alpha\beta} |U_{e3}|^2 |U_{\beta 3}|^2 \left(1 + \frac{4}{\Delta_{31}} sc - \frac{12}{\Delta_{31}^2} s^2\right) \\
& + 2|U_{e3}|^2 |U_{\beta 3}|^2 |U_{\alpha 3}|^2 \left(s^2 + \frac{6}{\Delta_{31}} sc - \frac{12}{\Delta_{31}^2} s^2\right) \\
& + 2\delta_{\alpha\beta} |U_{e3}|^4 |U_{\beta 3}|^2 \left(s^2 + \frac{6}{\Delta_{31}} sc - \frac{12}{\Delta_{31}^2} s^2\right) \\
& + |U_{e3}|^4 (\delta_{\alpha e} \delta_{\beta e} - \delta_{\alpha e} |U_{\beta 3}|^2 - \delta_{\beta e} |U_{\alpha 3}|^2) \left(4 - 6s^2 - \frac{28}{\Delta_{31}} sc + \frac{40}{\Delta_{31}^2} s^2\right) \\
& + 4|U_{e3}|^4 |U_{\beta 3}|^2 |U_{\alpha 3}|^2 \left(1 - 2s^2 - \frac{10}{\Delta_{31}} sc + \frac{16}{\Delta_{31}^2} s^2\right).
\end{aligned} \tag{A.13g}$$

Here we have used the abbreviations $s = \sin(\Delta_{31}/2)$ and $c \equiv \cos(\Delta_{31}/2)$.

The lengthy expression given in Eq. (A.13d) has the form

$$P(\nu_\alpha \rightarrow \nu_\beta) = C_1 \sin^2 \frac{\Delta_{31}}{2} + C_2 \sin \frac{\Delta_{31}}{2} \cos \frac{\Delta_{31}}{2} + C_3, \tag{A.14}$$

where the coefficients C_1 , C_2 , and C_3 are written in terms of the elements of the mixing matrix, the mass parameters, and Δ_m . The coefficient C_1 is $O(1)$ while C_2 is first order or higher, so that Eq. (A.14) reduces to a two-generation formula in the zeroth-order approximation. We factor out $\sin(\Delta_{31}/2)$ from the sum of sinusoidal functions and transform the sum of the sine and cosine terms into a single sine term as

$$P(\nu_\alpha \rightarrow \nu_\beta) = \sqrt{C_1^2 + C_2^2} \sin \frac{\Delta_{31}}{2} \sin \left(\frac{\Delta_{31}}{2} + C_4 \right) + C_3, \tag{A.15a}$$

$$C_4 = \arctan \frac{C_2}{C_1}, \tag{A.15b}$$

where we take $0 \leq C_4 \leq \pi$ for $C_2 \geq 0$ and $\pi < C_4 < 2\pi$ for $C_2 < 0$. We rewrite Eq. (A.15a) as

$$P(\nu_\alpha \rightarrow \nu_\beta) = \sqrt{C_1^2 + C_2^2} \sin^2 \left(\frac{\Delta_{31}}{2} + \frac{C_4}{2} \right) - \sqrt{C_1^2 + C_2^2} \sin^2 \frac{C_4}{2} + C_3, \quad (\text{A}\cdot\text{16})$$

which reproduces the form of Eq. (4.1a) with

$$A \equiv \frac{1}{4l} \sqrt{C_1^2 + C_2^2}, \quad \Theta \equiv \frac{\Delta_{31}}{2} + \frac{C_4}{2}, \quad B \equiv \frac{1}{4l} \left(C_3 - \sqrt{C_1^2 + C_2^2} \sin^2 \frac{C_4}{2} \right). \quad (\text{A}\cdot\text{17})$$

The expressions of Eqs. (4.1b), (4.1c), and (4.1d) are obtained from Eq. (A.17) by setting $\alpha = \mu$ and $\beta = e$ in C_1 , C_2 , C_3 , and C_4 and taking the terms up to the appropriate order.

Appendix B

— Validity of the Approximation —

We made use of approximate formulae for the oscillation probability in §4. We elucidate the requirements for these formulae to be valid.

The approximation we developed in Appendix A requires

$$\delta m_{31}^2 \gg a, \delta m_{21}^2, \quad (\text{B}\cdot\text{1})$$

$$\Delta_m \equiv \frac{aL}{2E} = 5.0 \times 10^{-1} \left(\frac{L}{1000 [\text{km}]} \right) \left(\frac{\rho}{2.6 [\text{g cm}^{-3}]} \right) \ll 1, \quad (\text{B}\cdot\text{2})$$

and

$$\begin{aligned} \Delta_{21}(E) &\equiv \frac{\delta m_{21}^2 L}{2E} \\ &= 2.1 \times 10^{-1} \left(\frac{\delta m_{21}^2}{8.2 \cdot 10^{-5} [\text{eV}^2]} \right) \left(\frac{L}{1000 [\text{km}]} \right) \left(\frac{E}{[\text{GeV}]} \right)^{-1} \ll 1. \end{aligned} \quad (\text{B}\cdot\text{3})$$

Since neutrino energy we consider in this paper is $E \approx E_{\text{peak},n} \approx |\delta m_{31}^2| L / [2(2n + 1)\pi]$, the conditions given in Eq. (B) are satisfied at least marginally for $L \sim (300 - 1500)\text{km}$.

We additionally simplified the expression by dropping higher-order terms of $\sin \theta_{13}$ taking account of its smallness as mentioned in §4. Taking account of the relation $\Delta_{21} < \Delta_m$, we dropped terms of $O(\sin^2 \theta_{13})$ in the coefficients of Δ_{21}^2 and of $\Delta_{21} \Delta_m$, as well as terms of $O(\sin^3 \theta_{13})$ in the coefficients of Δ_m^2 . This simplification is valid when the omitted terms are much smaller than the leading term which is of $O(\sin^2 \theta_{13})$, or explicitly when the following conditions are satisfied:

$$\frac{\Delta_{21}(E_{\text{peak},n})^2 \sin^2 \theta_{13}}{\sin^2 \theta_{13}} = 1.1 \times 10^{-2} \cdot (2n + 1)^2 \frac{\left(\frac{\delta m_{21}^2}{8.2 \cdot 10^{-5} [\text{eV}^2]} \right)^2}{\left(\frac{|\delta m_{31}^2|}{2.5 \cdot 10^{-3} [\text{eV}^2]} \right)^2} \ll 1, \quad (\text{B}\cdot\text{4})$$

$$\frac{\Delta_{21}(E_{\text{peak},n})\Delta_m \sin^2 \theta_{13}}{\sin^2 \theta_{13}} = 5.2 \times 10^{-2} \cdot (2n+1) \frac{\left(\frac{\delta m_{21}^2}{8.2 \cdot 10^{-5} [\text{eV}^2]}\right)}{\left(\frac{|\delta m_{31}^2|}{2.5 \cdot 10^{-3} [\text{eV}^2]}\right)} \quad (\text{B-5})$$

$$\times \left(\frac{L}{1000 [\text{km}]}\right) \left(\frac{\rho}{2.6 [\text{g cm}^{-3}]}\right) \ll 1,$$

and

$$\frac{\Delta_m^2 \sin^3 \theta_{13}}{\sin^2 \theta_{13}} = 2.5 \times 10^{-1} \cdot \sin \theta_{13} \left(\frac{L}{1000 [\text{km}]}\right)^2 \left(\frac{\rho}{2.6 [\text{g cm}^{-3}]}\right)^2 \ll 1. \quad (\text{B-6})$$

These inequalities are satisfied for allowed values of $\sin^2 2\theta_{13} < 0.19$.⁵⁾

References

- 1) B. T. Cleveland et al., *Astrophys. J.* **496** (1998), 505.
 Y. Fukuda et al. (Kamiokande Collaboration), *Phys. Rev. Lett.* **77** (1996), 1683.
 J. N. Abdurashitov et al. (SAGE Collaboration), *J. Exp. Theor. Phys.* **95** (2002), 181 [*Zh. Eksp. Teor. Fiz.* **122** (2002), 211].
 W. Hampel et al. (GALLEX Collaboration), *Phys. Lett. B* **447** (1999), 127.
 M. Altmann et al. (GNO Collaboration), *Phys. Lett. B* **616** (2005), 174.
 M. B. Smy et al. (Super-Kamiokande Collaboration), *Phys. Rev. D* **69** (2004), 011104.
 S. N. Ahmed et al. (SNO Collaboration), *Phys. Rev. Lett.* **92** (2004), 181301.
 B. Aharmim et al. (SNO Collaboration), *Phys. Rev. C* **72** (2005), 055502.
- 2) Y. Ashie et al. (Super-Kamiokande Collaboration), *Phys. Rev. Lett.* **93** (2004), 101801;
Phys. Rev. D **71** (2005), 112005.
 M. C. Sanchez et al. (Soudan 2 Collaboration), *Phys. Rev. D* **68** (2003), 113004.
 M. Ambrosio et al. (MACRO Collaboration), *Eur. Phys. J. C* **36** (2004), 323.
- 3) T. Araki et al. (KamLAND Collaboration), *Phys. Rev. Lett.* **94** (2005), 081801.
 E. Aliu et al. (K2K Collaboration), *Phys. Rev. Lett.* **94** (2005), 081802.
- 4) M. Apollonio et al. (CHOOZ Collaboration), *Eur. Phys. J. C* **27** (2003), 331.
- 5) W. M. Yao et al. (Particle Data Group), *J. of Phys. G* **33** (2006), 1.
- 6) F. Ardellier et al., hep-ex/0405032.
 J. Cao, *Nucl. Phys. Proc. Suppl.* **155** (2006), 229.
 M. Aoki et al., hep-ex/0607013.
- 7) Y. Itow et al. (The T2K Collaboration), hep-ex/0106019.
- 8) For recent studies, see, for example:
 S. Pascoli and S. T. Petcov, *Phys. Lett. B* **544** (2002), 239.
 A. de Gouvêa, J. Jenkins and B. Kayser, *Phys. Rev. D* **71** (2005), 113009 and references therein.
 H. Nunokawa, S. J. Parke and R. Zukanovich Funchal, *Phys. Rev. D* **72** (2005), 013009.
 S. Choubey and W. Rodejohann, *Phys. Rev. D* **72** (2005), 033016.
 S. T. Petcov and T. Schwetz, *Nucl. Phys. B* **740** (2006), 1.
 M. Lindner, A. Merle and W. Rodejohann, *Phys. Rev. D* **73** (2006), 053005.
 S. M. Bilenky, M. D. Mateev and S. T. Petcov, *Phys. Lett. B* **639** (2006), 312.
 H. Minakata, H. Nunokawa, S. J. Parke and R. Zukanovich Funchal, *Phys. Rev. D* **74** (2006), 053008.
- 9) A. Cervera, A. Donini, M. B. Gavela, J. J. Gomez Cadenas, P. Hernández, O. Mena and S. Rigolin, *Nucl. Phys. B* **579** (2000), 17 [Errata; **593** (2001), 731].
 M. Koike, T. Ota and J. Sato, *Phys. Rev. D* **65** (2002), 053015.
 J. Pinney and O. Yasuda, *Phys. Rev. D* **64** (2001), 093008.
- 10) M. Koike, N. Okamura, M. Saito and T. Takeuchi, *Phys. Rev. D* **73** (2006), 053010.
- 11) J. Burguet Castell, M. B. Gavela, J. J. Gómez Cadenas, P. Hernández and O. Mena, *Nucl. Phys. B* **608** (2001), 301.
- 12) H. Minakata and H. Nunokawa, *J. High Energy Phys.* **10** (2001), 001.
 H. Minakata, H. Nunokawa and S. J. Parke, *Phys. Lett. B* **537** (2002), 249.

- 13) G. L. Fogli and E. Lisi, Phys. Rev. D **54** (1996) 3667.
- 14) M. Freund, P. Huber and M. Lindner, Nucl. Phys. B **615** (2001), 331.
P. Huber, M. Lindner and W. Winter, Nucl. Phys. B **645** (2002), 3.
H. Minakata, H. Nunokawa and S. J. Parke, Phys. Rev. D **66** (2002), 093012.
J. Burguet-Castell, M. B. Gavela, J. J. Gómez-Cadenas, P. Hernández and O. Mena, Nucl. Phys. B **646** (2002), 301.
P. Huber, M. Lindner, M. Rolinec, T. Schwetz and W. Winter, Phys. Rev. D **70** (2004), 073014.
O. Mena and S. J. Parke, Phys. Rev. D **70** (2004), 093011.
A. Donini, E. Fernandez-Martinez and S. Rigolin, Phys. Lett. B **621** (2005), 276.
P. Huber, M. Lindner and W. Winter, J. High Energy Phys. **05** (2005), 020.
P. Huber, M. Maltoni and T. Schwetz, Phys. Rev. D **71** (2005), 053006.
- 15) Y. F. Wang, K. Whisnant, Z. h. Xiong, J. M. Yang and B. L. Young (VLBL Study Group H2B-4), Phys. Rev. D **65** (2002), 073021.
M. Aoki, K. Hagiwara, Y. Hayato, T. Kobayashi, T. Nakaya, K. Nishikawa and N. Okamura, Phys. Rev. D **67** (2003), 093004.
K. Whisnant, J. M. Yang and B. L. Young, Phys. Rev. D **67** (2003), 013004.
V. Barger, D. Marfatia and K. Whisnant, Phys. Lett. B **560** (2003), 75.
M. Ishitsuka, T. Kajita, H. Minakata and H. Nunokawa, Phys. Rev. D **72** (2005), 033003.
K. Hagiwara, N. Okamura and K. i. Senda, Phys. Lett. B **637** (2006), 266 [Errata; **641** (2006), 486].
T. Kajita, H. Minakata, S. Nakayama and H. Nunokawa, Phys. Rev. D **75** (2007), 013006.
O. Mena, H. Nunokawa and S. J. Parke, Phys. Rev. D **75** (2007) 033002.
- 16) V. Barger, D. Marfatia and K. Whisnant, Phys. Rev. D **65** (2002), 073023.
- 17) A. Aguilar et al. (LSND Collaboration), Phys. Rev. D **64** (2001), 112007.
- 18) B. Armbruster et al. (KARMEN Collaboration), Phys. Rev. D **65** (2002), 112001.
- 19) A. A. Aguilar-Arevalo *et al.* (The MiniBooNE Collaboration), Phys. Rev. Lett. **98** (2007), 231801.
- 20) M. V. Diwan et al., Phys. Rev. D **68** (2003), 012002.
- 21) J. Arafune, M. Koike and J. Sato, Phys. Rev. D **56** (1997), 3093 [Errata; **60** (1999), 119905].
M. Koike and J. Sato, Mod. Phys. Lett. A **14** (1999), 1297; Phys. Rev. D **61** (2000), 073012 [Errata; **62** (2000), 079903].